Environmental Science and Ecotechnology 14 (2023) 100225

Contents lists available at ScienceDirect

Environmental Science and Ecotechnology

journal homepage: www.journals.elsevier.com/environmental-science-and-ecotechnology/

Original Research

Iron species activating chlorite: Neglected selective oxidation for water treatment

Qihui Xu [a], Zhipeng Li [b], Feng Liu [b], Hong You [a, b, *], Binghan Xie [a, b, **]

[a] State Key Laboratory of Urban Water Resources and Environment, Harbin Institute of Technology, Harbin, 150090, China
[b] School of Marine Science and Technology, Harbin Institute of Technology at Weihai, Weihai, 264209, China

ARTICLE INFO

Article history:
Received 15 July 2022
Received in revised form
13 November 2022
Accepted 14 November 2022

Keywords:
Iron species
Chlorite
High-valent-Fe-oxo
Chlorine dioxide
Coordination catalysis

ABSTRACT

Chlorite (ClO_2^-) is the by-product of the water treatment process carried out using chlorine dioxide (ClO_2) as an effective disinfectant and oxidant; however, the reactivation of ClO_2^- has commonly been overlooked. Herein, it was unprecedentedly found that ClO_2^- could be activated by iron species (Fe_b: Fe^0, Fe^{II}, or Fe^{III}), which contributed to the synchronous removal of ClO_2^- and selective oxidative treatment of organic contaminants. However, the above-mentioned activation process presented intensive H^+-dependent reactivity. The introduction of Fe_b significantly shortened the autocatalysis process via the accumulation of Cl^- or ClO^- during the protonation of ClO_2^- driven by ultrasonic field. Furthermore, it was found that the interdependent high-valent-Fe-oxo and ClO_2, after identification, were the dominant active species for accelerating the oxidation process. Accordingly, the unified mechanisms based on coordination catalysis ($[Fe^N(H_2O)_a(ClO_x^{m-})_b]^{n+}$-P) were putative, and this process was thus used to account for the pollutant removal by the Fe_b-activated protonated ClO_2^-. This study pioneers the activation of ClO_2^- for water treatment and provides a novel strategy for "waste treating waste". Derivatively, this activation process further provides the preparation methods for sulfones and ClO_2, including the oriented oxidation of sulfoxides to sulfones and the production of ClO_2 for on-site use.

1. Introduction

Chlorite (ClO_2^-), as a redox agent with wide application prospects, can be used not only as an alkaline Cl oxidant with a high oxidation capacity [1] but also as a source of chlorine dioxide (ClO_2) via electron loss [2] (e.g., ultraviolet (UV) activation [3]). As a selective oxidant, the produced ClO_2 could be considered a stable radical species which is significantly reactive toward phenolic, aniline, olefin, and amine moieties through electron-transfer reactions [4]. Moreover, ClO_2 was used as a strong disinfectant in water treatment plants, which acted as an alternative to chlorine [5,6]. It was also found that ClO_2 was the most efficient disinfectant in killing bacteria and, in particular, successful in deactivating viruses over a wide pH range [7]. However, ClO_2^- has been seen as the by-product of ClO_2 treatment, and the Environmental Protection Agency has recently labeled ClO_2^- as a major water contaminant. ClO_2^- could result in suspected health risks such as childhood anemia [2]. According to "Standards for drinking water quality, GB5749-2022" in China, the limited concentration of ClO_2^- after ClO_2 disinfection was reported to be 0.7 mg L^{-1} [8]. Therefore, a method to remediate ClO_2^- is of great practical interest from an environmental standpoint [2].

Currently, the catalysts, including various chlorite-dismutases (e.g., Fe^{III}-Clds) [9–12] or non-heme metalloporphyrins/metal complexes (e.g., Mn^{III}-Pors) [13–18], are also utilized to catalyze ClO_2^- detoxification, which results in the formation of harmless chloride (Cl^-) and dioxygen (O_2) [9–15] or ClO_2 [16–18]. Moreover, the corresponding trivalent metal (M^{III}) gets transformed into high-valent metal (HVM), $O{=}M^{IV}$, or $O{=}M^{IV\bullet+}$ [9–18].

Recently, in advanced oxidation processes (AOPs), the formation and role of aqueous Fe^{IV}-oxo complex ($Fe^{IV}O^{2+}$) have also attracted significant research attention in ferrous ion (Fe^{2+})-initiated AOPs by employing the oxidants including ozone, hydrogen peroxide, persulfates, peracetic acid (PAA), etc. [19]. Compared to the long-

* Corresponding author. State Key Laboratory of Urban Water Resources and Environment, Harbin Institute of Technology, Harbin, 150090, China.
** Corresponding author. State Key Laboratory of Urban Water Resources and Environment, Harbin Institute of Technology, Harbin, 150090, China.
E-mail addresses: youhong@hit.edu.cn (H. You), xiebinghan@hit.edu.cn (B. Xie).

https://doi.org/10.1016/j.ese.2022.100225

recognized free radicals, $Fe^{IV}O^{2+}$ has been shown to remove various pollutants (e.g., phosphite, amoxicillin, and sulfamethoxazole) [19,20]. Moreover, $Fe^{IV}O^{2+}$ could react with organic compounds through various pathways (hydrogen-atom, hydride, oxygen-atom, and electron transfer, as well as electrophilic addition) at moderate reaction rates [19]. $Fe^{IV}O^{2+}$ could also present selective reactivity toward inorganic ions prevailing in natural water [19]. This hints at the potential application prospects of high-valent iron in environmental treatment due to the production of the above-mentioned HVM in the catalysis of ClO_2^-.

$$4Fe^{2+} + ClO_2^- + 10H_2O \xrightarrow{OH^-} 4Fe(OH)_3(s) + Cl^- + 8H^+ \quad (1)$$

In terms of the reactions between ionic iron and ClO_2^-, Fe^{II} was commonly adopted to reduce ClO_2^- to form the by-product Cl^- (95%) [21], in particular, under the alkaline condition for efficient ClO_2^- removal (as shown in equation (1)) [21,22]. However, a few studies indicated that the different phenomenon with a certain catalytic effect between ionic iron and ClO_2^- was observed under acidic conditions, which could be analogous to the conventional Fenton reaction. For instance, Fe^{III} could catalyze the decomposition of ClO_2^- to generate ClO_2 [23]. Fabian and Gordon considered the formation of $FeClO_2^{2+}$-intermediates during the catalytic process (equation (2)) [24–27]. Nevertheless, compared with the above-mentioned catalytic activity of metalloporphyrin, it seemed that the catalytic mechanism of producing ClO_2 further demands a lot more systematic explorations and improvement on the conversion of intermediate active substances, such as whether it could relate to the role of $Fe^{IV}O^{2+}$.

$$Fe^{3+} + ClO_2^- \leftrightarrow FeClO_2^{2+} \leftrightarrow Fe^{2+} + ClO_2 \quad (2)$$

Noteworthy, the previous studies were limited to the detoxification of ClO_2^- via its decomposition. However, the potential water treatment was neglected by producing $Fe^{IV}O^{2+}$ or ClO_2 with a significant oxidation effect under the detoxification process. Therefore, based on the treatment of organic pollutants with by-product ClO_2^- via activation by iron species (Fe_b), the strategy for simultaneous removal of ClO_2^- and selective removal of organic pollutants was provided. However, to the best of our knowledge, this topic has rarely been investigated to date.

Therefore, the objectives of this study include reporting the novel methods and corresponding mechanisms of applying Fe_b (e.g., $Fe^{0,\ II,\ or\ III}$)-activated ClO_2^- under protonation by ultrasonic in the water treatment process. The ultrasonic was adopted as the field driving the diffusion. On the one hand, the study focused on the process of activating ClO_2^- with Fe^0 for the synchronous removal of ClO_2^- and triphenylmethane (tpm) derivatives. On the other hand, the activation mechanisms of Fe^0-activated ClO_2^- including the contributions of the dominant active species for pollutant removal were further modified and elucidated. Briefly, this study may provide a novel insight into the coordination mechanism in ClO_2^- activated by Fe_b, and further offer an insightful strategy for "waste treating waste".

2. Experimental

2.1. Materials

Fe-based materials including Fe^0, Fe^{II}, and Fe^{III} species were selected, i.e., zero-valent-iron foam (Fe^0_f), iron(II) sulfate heptahydrate ($FeSO_4 \cdot 7H_2O$), and iron(III) chloride hexahydrate $FeCl_3 \cdot 6H_2O$, respectively. Sodium chlorite ($NaClO_2$ (CI), 80%) and crystal violet (tpm_{CV}), a type of tpm derivative, were obtained from Macklin. Other chemicals, including commercially available analytical grade methyl phenyl sulfoxide (PMSO), dimethyl sulfoxide (DMSO), anions such as Na-salts (Cl^-, SO_4^{2-}, and CO_3^{2-}), sodium azide (NaN_3), *p*-benzoquinone (PBQ), methyl alcohol (MA), ethylene-diamine-tetraacetic acid (EDTA), and oxalic acid ($H_2C_2O_4$), were used without further purification. All reactions were carried out in deionized water obtained using a Heal Force water purification system (SMAR-RO).

2.2. Instrumentation

The liquid phase reactions were driven by ultrasound (US) in a self-prepared bath-ultrasonic generator (28 kHz, 30 W L^{-1}) coupled with a cylindrical acrylic reactor, as reported in our previous study [28]. The tpm_{CV} solution (12 mg L^{-1}) was prepared and placed in the above-mentioned reactor. Briefly, certain amounts of H_2SO_4, $NaClO_2$, and Fe^0_f were added successively, and then the ultrasonic reactor was turned on to conduct the batch reaction. At the fixed reaction time, the tpm_{CV} concentration was determined at $\lambda_{max} = 584$ nm by UV–visible (vis) spectroscopy. The initial pH of solutions was adjusted by NaOH (1 M) and H_2SO_4 (1 M), and no attempt was made to maintain a constant pH during the process. UV–vis spectra were recorded using a scanning spectrophotometer (Pgeneral TU-1810S). The converted products of PMSO were detected by gas chromatograph-mass spectrometry (GC/MS, Trace 1300 ISQ-QD, Thermo Fisher). Before the GC/MS analysis, a subsample (15 mL) at a certain treating time (5, 15, and 25 min) was extracted with dichloromethane (10 mL), respectively. Next, the extracted solution was dehydrated with anhydrous sodium sulfate and concentrated to 2 mL. Before and after treatment, the micrographs of the Fe^0_f were examined by scanning electron microscopy (SEM, Zeiss, Germany), respectively. Before the SEM test, the Fe^0_f samples taken out from the reaction solution immediately required dehydration by adding absolute ethyl alcohol, then the samples were dried with filter papers and finally vacuum-dried.

3. Results and discussion

3.1. Fe_b activation for chlorite

3.1.1. Coupling effect

As shown in Fig. 1a, activators including Fe^0, Fe^{II}, and Fe^{III} were utilized to catalyze the decomposition of ClO_2^- for removing tpm_{CV} at acidic pH under the ultrasonic field. The tpm_{CV}, as the emerging contaminant, has been widely used in medical, veterinary, and aquaculture applications. However, the "*Lancet Oncology*" reported that tpm_{CV} had been restricted in veterinary or cosmetic applications [29]. The system exhibited a coupling effect; namely, removal effect in the following: $Fe^{III} > Fe^{II} > Fe^0 >$ no activator. The apparent second-order kinetics constants of the H^+-US/CI/Fe^{II} and H^+-US/CI/Fe^{III} systems were 0.043 μM^{-1} min^{-1} ($R^2_{Adj} = 0.996$) and 0.115 μM^{-1} min^{-1} ($R^2_{Adj} = 0.995$), respectively. When the H^+-US/CI/Fe^0 system was utilized, Fe^0, in the presence of H^+, could be converted to Fe^{II}, and Fe^{II} could be further oxidized into Fe^{III} via equations (3) and (4) [27,30]. Next, Fe^{III} could catalyze ClO_2^- to produce reactive species for decomposing ClO_2^- and tpm_{CV}. For the H^+-US/CI system, ClO_2^- could react with H^+ to generate ClO_2 via equation (5) [31], and then protonated ClO_2^- formed $HClO_2$, which was subjected to sonolysis to produce ClO_2. In terms of the H^+-US/CI and H^+-US/CI/Fe^0 systems, both the removal processes exhibited an early stage of "build-up". Based on the dynamics fitting, the piecewise kinetics of the above-mentioned systems (Fig. 1b) proved this point.

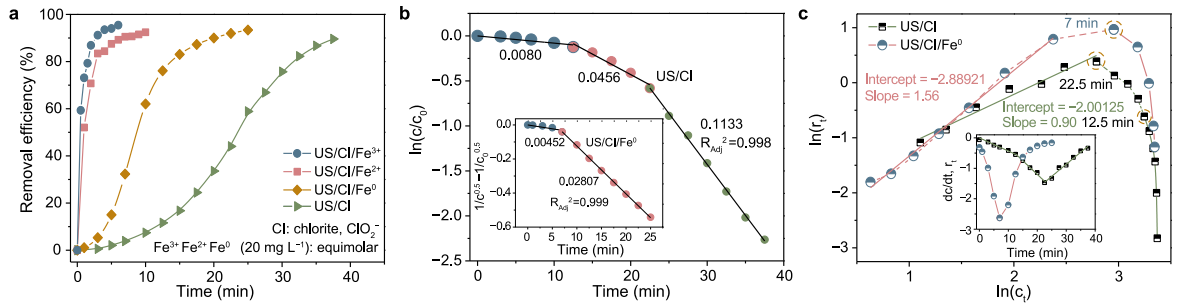

Fig. 1. Fe-based activation for chlorite (ClO_2^-) by virtue of protonation (H^+): **a**, system comparison; **b**–**c**, piecewise kinetics; tpm_{CV} (12 mg L^{-1}), US (30 W L^{-1}, 28 kHz), ClO_2^- dosage (3 mM), 1 M H_2SO_4 (0.2 mL L^{-1}), vortex (0 rad min^{-1}), and initial T (293 K).

$$5Fe^{2+} + ClO_2 + 4H^+ \rightarrow Cl^- + 5Fe^{3+} + 2H_2O \quad (3)$$

$$4Fe^{2+} + HClO_2 + 3H^+ \rightarrow Cl^- + 4Fe^{3+} + 2H_2O \quad (4)$$

$$5ClO_2^- + 4H^+ \rightarrow Cl^- + 4ClO_2 + 2H_2O \quad (5)$$

3.1.2. Piecewise kinetics: transition state

Owing to the removal reaction presenting an "S"-process, namely, existing transition state, traditional one-step dynamics with integer order failed to meet the requirement of exploring such piecewise oxidation stages. Fortunately, equation (6) is universal, that is

$$\frac{d[tpm_{CV}]}{dt} = f'(c_{tpm_{CV}}) \quad (6)$$

Multiple inflection points (IPs) directly obtained from the process of "dc/dt vs. t" further indicated the existence of the piecewise kinetics processes for both H^+-US/CI and H^+-US/CI/Fe^0 systems (Fig. 1c). After logarithmic transformation, the apparent-kinetics-orders (non-integer) of the H^+-US/CI and H^+-US/CI/Fe^0 systems were 0.90 and 1.56, respectively.

Moreover, in view of excess active oxidizing species (3 mM ClO_2^- >> 30 μM tpm_{CV}), equation (7) could be obtained.

$$f'(c_{tpm_{CV}}) = -kc_{tpm_{CV}}{}^n \quad (7)$$

Then, by feasible approximation, the piecewise kinetics processes were more obvious when 1 and 1.5 orders were utilized to fit kinetics curves of the H^+-US/CI and H^+-US/CI/Fe^0 systems, respectively (Fig. 1b).

According to the H^+-US/CI system, two IPs at 12.5 and 22.5 min indicated the existence of three piecewise removal processes. Moreover, processes occurring in the time range of 0–12.5 min and 12.5–22.5 min with slow reaction rates indicated the potential autocatalytic feasibility, and the reaction at 22.5–37.5 min showed pseudo-1-order kinetics constant with a value of 0.113 min^{-1}. After introducing Fe^0, the time of the stage of "build-up", namely, IP was shortened to 7 min, and 7–25 min exhibited pseudo-1.5-order kinetics constant with a value of 0.056 $\mu M^{-0.5}$ min^{-1}, which indicated that non-single oxidizing-species contributed to the pollutant removal. As a result, it is speculated that multiple oxidizing species may compete for the oxidation process.

3.1.3. Surface action by US

As shown in Fig. 2, SEM images showed more features with a relatively large size (20 μm), such as the honeycomb frame and the oxidation regions. With the prolongation of reaction time, the erosion and oxidation on the surface of Fe^0-foam became more significant. Even so, most regions on surface of Fe^0-foam still consisted of exposed fresh Fe^0 sources due to the "polishing" role from ultrasonic via surface heat transfer, mechanical friction, and cavitation impact [28]. Owing to the synergistic effect between H^+-assisted corrosion and ultrasonic-assisted polishing, the catalytic reaction of ClO_2^- could be sustained.

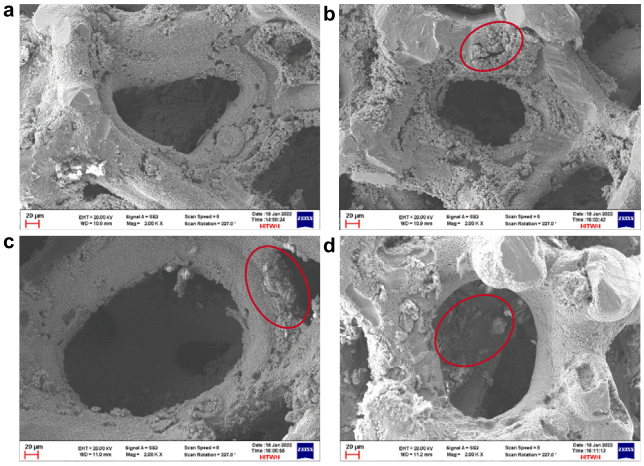

Fig. 2. Surface morphology of Fe^0-foam under H^+-US/CI at different treating times: **a**, 0 min; **b**, 5 min; **c**, 15 min; **d**, 25 min.

3.1.4. Modeling

Complex reactions tended to multistage processes during the heterogeneous system (i.e., the abovementioned system) at a certain treating time. It may be unsuitable to describe reaction processes under overall evaluation only with a single quasi-dynamic equation. Here, a novel indicator was used to evaluate the removal effect in a heterogeneous system. In particular, at a certain time, the degraded momentum, namely, the concentration movement of removing contaminant μ (M min M^{-1}), could be defined to determine the overall trends of the removal [32].

$$\mu = \int_{t_0}^{t_e} \frac{c_0 - c_t}{c_0} t \quad (8)$$

where c_t/c_0 was the concentration gradient of contaminant ($c_t/c_0 \in [0,1]$), t_0 and t_e represented the start and end times of the reaction. Theoretically, the value μ_{max} equals the value t_e, namely, c_t/c_0 reached 0 at t_0.

$$r_{app} = \frac{\mu}{\mu_{max}} \quad (9)$$

where r_{app} was the apparent ratio of concentration movement.

$$\varphi = \frac{r_{app_i}}{r_{app_{con}}} \quad (10)$$

where φ was the relative factor, i represented one influencing factor, and con represented the control group. Moreover, the t_e was selected at 17.5 or 22.5 min in the follow-up evaluation.

3.2. Influencing factors

3.2.1. pH

As shown in Fig. 3a, the removal reaction could be improved by introducing H^+ into the H^+-US/CI/Fe^0 system (φ increased from 0.856 to 1.331). H^+ could cause the conversion of Fe^0 to ionic Fe for activation. However, once the system presented a neutral or basic state, it became fatal to Fe^0-activation. The abovementioned system was close to only US/CI or OH^--US/CI, leading to a very limited oxidation effect. However, it seemed that the removal effect under alkaline conditions ($\varphi = 0.119$) was slightly better than that under neutral conditions ($\varphi = 0.090$). The sonolysis of ClO_2^- could generate reactive radicals (e.g., $\bullet ClO_x^{n-}$), which was supported by our previous study [28]. Photolysis of ClO_2^- was ever investigated to obtain that OH^- was found to be conducive to the transformation of free radicals [1], which may be analogous to the above-mentioned result. Moreover, OH^- may prevent the organic substances from evaporating into the cavitation bubble for pyrolysis, leading to the occurrence of the free radical oxidation only at the gas–liquid interface of the cavitation bubble.

3.2.2. ClO_2^- dosage

The solution produces OH^- due to the hydrolysis of ClO_2^- [33]. More ClO_2^- dosage leads to the generation of more OH^-, which can increase the consumption of H^+. As a result, the amount of H^+ actually acting on Fe^0 and ClO_2^- decreases. However, more reactant ClO_2^- could bring more effective collisions and improved utilization efficiency of other reactants (e.g., H^+). The removal reaction in system H^+-US/CI/Fe^0 maintained a balance (Fig. 3b) (φ around 0.959–1.008).

3.2.3. Anions

The anions, including SO_4^{2-} ($\varphi = 0.981$) and Cl^- ($\varphi = 1.002$) (3 mM), would not interfere with the solution-phase oxidation; however, CO_3^{2-} (1 mM) exhibited significant influence on the removal of tpm_{CV} (Fig. 3c) in the H^+-US/CI/Fe^0 system ($\varphi = 0.140$). The main reason for the phenomenon was that the formation of OH^- via hydrolysis of CO_3^{2-} (equation (11)) resulted in competitive consumption of H^+ [34]. Furthermore, OH^- led to the formation of the colloidal or precipitated $Fe(OH)_n$, which adversely affected the activation of ClO_2^- with Fe^{n+}. Therefore, low-dosage CO_3^{2-} (0.1 mM) showed a slight influence on removing tpm_{CV} ($\varphi = 0.837$), which indicated that the reaction was not interfered with by the ions themselves except the hydrolysis.

$$H_2CO_3 \overset{pKa=6.34}{\Leftrightarrow} H^+ + HCO_3^- \overset{pKa=10.37}{\Leftrightarrow} 2H^+ + CO_3^{2-} \quad (11)$$

3.3. Inhibition

The reaction rate of MA vs. •OH was 9.7×10^8 M^{-1} s^{-1}; therefore, MA could be used as a scavenger for •OH [35]. However, when MA (1 M) was added to the solution, the removal trend seemed to remain constant ($\varphi = 0.982$) (Fig. 4a). Therefore, the •OH (at least in the liquid phase) showed little contribution to the removal of tpm_{CV}, illustrating that ultrasonic provided other roles rather than •OH role in the catalytic system.

Notably, DMSO has recently been used to identify oxygen atom transfer reactions, such as reaction with $Fe^{IV}O^{2+}$ to form $DMSO_2$ (equation (12)) [36]. However, DMSO could also react with •OH to generate methyl radical ($\bullet CH_3$) (equation (13)) [37].

$$Fe^{IV}O^{2+} + DMSO \rightarrow DMSO_2 + Fe^{2+} \quad (12)$$

$$\bullet OH + DMSO \rightarrow \bullet CH_3 + CH_3SO_2H \quad (13)$$

The screening test of MA ruled out the role of •OH; thus, the decrease in the removal of tpm_{CV} after adding DMSO should be attributed to the active species causing an oxygen atom ([O]) transfer step. Moreover, it was demonstrated that DMSO could be an excellent masking agent for aqueous chlorine (e.g., Cl_2 or ClO^- (HClO)), without affecting ClO_2, ClO_2^-, and ClO_3^- by the co-existence of excess DMSO [30,38,39].

PBQ could be used to scavenge superoxide radical ($O_2^{\bullet -}$) with a reaction rate at 8×10^9 M^{-1} s^{-1} [40], but the result indicated the

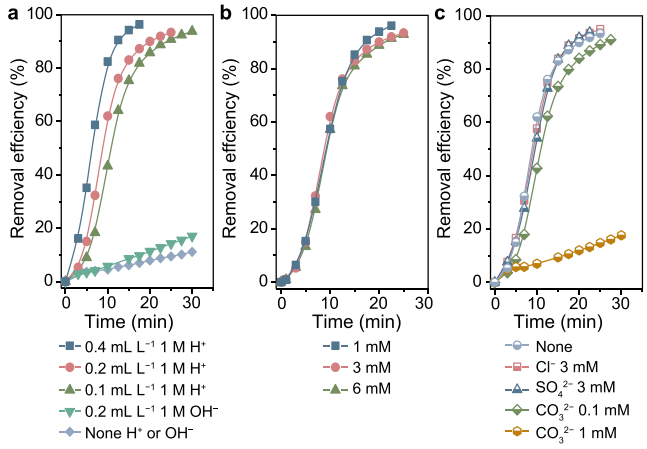

Fig. 3. Influencing factors for H^+-US/CI/Fe^0 system: **a**, pH; **b**, ClO_2^- dosage; **c**, anion. Conditions ibid., Fig. 1.

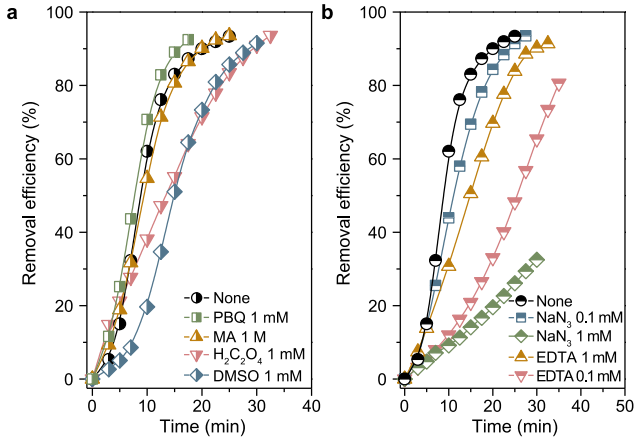

Fig. 4. Possible inhibition (**a**), competition and coordination (**b**) from two reactants for H^+-US/CI/Fe^0 system. Conditions ibid., Fig. 1.

absence of $O_2^{\bullet-}$ and the addition of PBQ appeared to promote the removal of tpm_{CV} (φ = 1.159) (Fig. 4a). The PBQ acted as an important redox reagent. Its applications range from organic synthesis to mediation of electron transfer in biochemical systems and solar cells [41]. On the one hand, the PBQ-based derivatives with electron-withdrawing substituents were employed as electron acceptors, and the quinones could serve as catalysts to shuttle electrons; thus, both facilitated the degradation of the starting aromatic compound [42]. On the other hand, the mixing of solutions of halide anions (I^-, Br^-, or Cl^-) with PBQ acceptors resulted in the instantaneous formation of anion−π complexes [41]. This pointed out the charge-transfer character of these associates (equation (14)) [41].

$$BQ + X^- \leftrightarrow BQ^{\bullet-} + X^{\bullet} \quad (14)$$

3.4. Competition and coordination

Oxalic acid and EDTA, as the chelating agents for metal ions, bonded with Fe^{n+}, which impeded Fe^{n+}-induced activation of ClO_2^- (Fig. 4). Oxalic acid could react with Fe^{n+} to form some complexes, i.e., $[Fe^{III}(C_2O_4)_n]^{3-2n}$ and $[Fe^{II}(C_2O_4)_n]^{2-2n}$ [43], leading to the competing reaction (φ = 0.756). In particular, EDTA could combine with $[Fe^{II/III}(H_2O)_6]^{2+/3+}$ to form the coordination complex. For instance, $[Fe^{II}(EDTA)H_2O]^{2-}$ was the seven-coordinated species with a monocapped trigonal-prismatic geometry [44]. On acidification, EDTA chelate could be protonated to form a monoprotonated species $[Fe^{II}(EDTAH)H_2O]^-$ with pentagonal−bipyramidal geometry [44]. The autoxidation of $[Fe^{II}(EDTA)]$: the $[Fe^{II}(EDTA)H_2O]^{2-}$ (20-electron) could start the reaction with O_2 to form H_2O_2, and the reaction was controlled by electron transfer and the associated reorganization barrier. The reactions were presented as equations (15)–(20) [44]. Thus, with the increase in the EDTA dosage, the autoxidation effect surpassed the metal chelation effect, resulting in promoting the removal (φ increased from 0.291 to 0.666). Furthermore, more EDTA resulted in the decrease of the pH of the solution, which was also beneficial for the removal (Fig. 4b).

$$Fe^{2+} + EDTA \rightarrow \left[Fe^{II}(EDTA)\right] \xrightarrow{H_2O} \left[Fe^{II}(EDTA)H_2O\right]^{2-} \quad (15)$$

$$\left[Fe^{II}(EDTA)H_2O\right]^{2-} + H^+ \leftrightarrow \left[Fe^{II}(EDTAH)H_2O\right]^- \quad (16)$$

$$\left[Fe^{II}(EDTAH)H_2O\right]^- + O_2 \leftrightarrow \left[Fe^{II}(EDTAH)O_2\right]^- + H_2O \quad (17)$$

$$\left[Fe^{II}(EDTAH)O_2\right]^- \rightarrow \left[Fe^{III}(EDTAH)O_2^-\right]^- \quad (18)$$

$$\left[Fe^{II}(EDTAH)H_2O\right]^- + \left[Fe^{III}(EDTAH)O_2^-\right]^- \rightarrow \left[(EDTAH)Fe^{III}\left(O_2^{2-}\right)Fe^{III}(EDTAH)\right]^{2-} + H_2O \quad (19)$$

$$\left[(EDTAH)Fe^{III}\left(O_2^{2-}\right)Fe^{III}(EDTAH)\right]^{2-} \xrightarrow[H_2O]{H^+} 2\left[Fe^{III}(EDTAH)H_2O\right] + H_2O_2 \quad (20)$$

When NaN_3 was used (Fig. 4b), the study reported that without spin trap agent *N-tert*-butyl-α-phenylnitrone, the reaction of ClO_2 with azide (N_3^-) was strongly inhibited by ClO_2^- due to rapid back-electron transfer. This led to additional mechanistic pathways, complex kinetics, and the formation of an unusual set of products, including N_2, N_2O, NO_3^-, Cl^-, and ClO_2^- as represented in equations (21)–(26) [45]. Furthermore, in the presence of an iron(III)-azide system, the complex formation reaction occurred via the conjugate acid/conjugate base pathway (equation (27)) [46].

$$ClO_2 + N_3^- \leftrightarrow N_3 + ClO_2^- \quad (21)$$

$$N_3 + PBN \rightarrow PBNN_3 \quad (22)$$

$$10ClO_2 + 10N_3^- + 4H_2O \rightarrow 10Cl^- + 8NO_3^- + 11N_2 + 8H^+ \quad (23)$$

$$8ClO_2 + 8N_3^- + H_2O \rightarrow 8Cl^- + 2NO_3^- + 11N_2O + 2H^+ \quad (24)$$

$$2ClO_2 + 2N_3^- \rightarrow 2ClO_2^- + 3N_2 \quad (25)$$

$$ClO_2 + N_3^- + 0.278H_2O \rightarrow 0.833Cl^- + 0.167ClO_2^- + 0.555NO_3^- + 0.278N_2O + 0.943N_2 + 0.555H^+ \quad (26)$$

$$Fe(H_2O)_5OH^{2+} + HN_3 \rightarrow Fe(H_2O)_5N_3^{2+} + H_2O \quad (27)$$

The above-mentioned competitive competition and coordination reaction indicated the occurrence of a transfer process from primary reactants (ClO_2^- and Fe^0) to secondary reactants (ClO_2 or Fe^{n+}). The deprivation of ClO_2 or Fe^{n+} led to poor removal performance, demonstrating the enhancement of effective active species around them.

3.5. Mechanism discussion

3.5.1. Identification

The identification of active species involved the investigation of Cl-containing species and Fe-containing species. The ClO_2^- was consumed at 260 nm (ε = 154 M^{-1} cm^{-1}) [16–18], and the formation of ClO_2 was monitored by the characteristic absorption band at 360 nm (ε = 1200 M^{-1} cm^{-1}) [2,16–18] with a width at half-maximum of about 80 nm. The spectrum was unusual for the condensed phase in that it showed a vibrational structure, making this a very characteristic spectrum [40]. Moreover, the introduction of Fe^0 made the production of ClO_2 extremely pronounced (Fig. 5b and c). Based on the measurement of ClO_2 concentrations at 360 nm, the ClO_2 produced by the H^+-US/CI system exhibited linear relation with the action time, i.e., $A_{360\ nm} = 0.00443t_{min}$ ($R^2_{Adj} > 0.999$) (Fig. 5a). However, the generation of ClO_2 in the H^+-US/CI/Fe^0 system, in contrast, increased rapidly. This could explain why the apparent activation of the H^+-US/CI/Fe^0 system was more effective from a certain perspective. Moreover, the studies reported that λ at around 290 nm was responsible for the presence of chlorine (as ClO^-) [47,48], and the corresponding λ could be detected for both the H^+-US/CI and H^+-US/CI/Fe^0 systems with the hidden absorption.

Recently, PMSO has been used as a chemical probe to identify $Fe^{IV/V}$-oxo (HVI-oxo) species by turning itself into sulfones ($PMSO_2$) due to the aforementioned [O] transfer process. However, noteworthy, it was important to discuss whether PMSO was suitable for HVI-oxo identification. The studies reported that RMSO (e.g., DMSO) could mask aqueous chlorine (e.g., Cl_2 or ClO^-) [38,39]; however, Cl-containing species by identification were ClO_2 (the difference was obvious after the introduction of Fe^0) in this study. Except under specific catalysts, the ClO_2 showed a limited ability to directly oxidize sulfoxides to sulfones [49,50]. Unlike sulfide

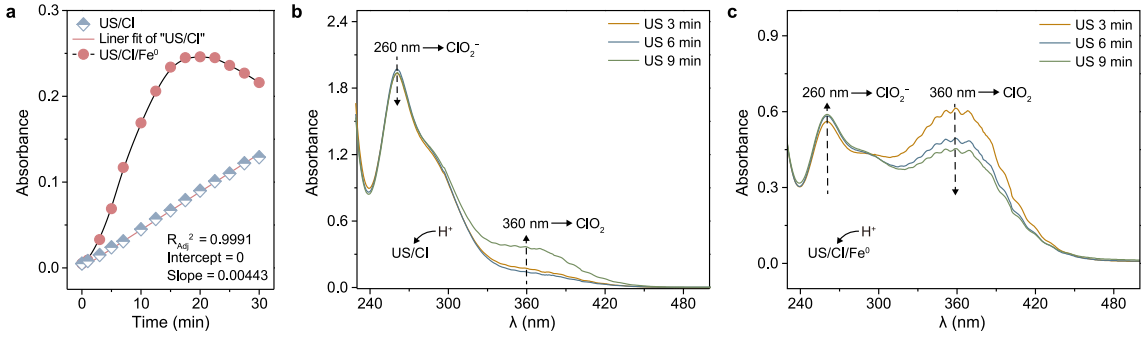

Fig. 5. UV–vis spectroscopy for the ClO_2^- and ClO_2 during catalysis/activation: **a**, concentration variation at 360 nm; **b**, H^+-US/CI system; **c**, H^+-US/CI/Fe^0 system. Conditions: **a**, ibid., Fig. 1; **b**–**c**, Fe^0_f (80 mg L^{-1}), CI (12 mM), 1 M H_2SO_4 (0.8 mL L^{-1}). Detection: **a**–**b**, undiluted; **c**, diluted, sample:water (1:2, v/v); **b**–**c**, detection time (30 min).

oxidation processes, part of the sulfones was generated [49]. Therefore, by elimination process, the ClO^- was also likely to cause the generation of $PMSO_2$. As a result, this might be a good explanation for why a small amount of $PMSO_2$ (retention time (t_R) = 9.27 min, *m/z* of 156, 141, 125, 94, and 77) was detected by GC/MS (Fig. 6), and the remaining most PMSO (t_R = 8.43 min, *m/z* of 140, 125, 97, and 77) was present in the H^+-US/CI system. Then the introduction of Fe^0 led to the production of $PMSO_2$ in large quantities (Fig. 6), which should be attributed to HVI-oxo species due to the (relatively stable) imperceptible change in ClO^- after Fe-activation. Briefly, the [O] of newly formed $PMSO_2$ was derived from ClO_2^- rather than from $\cdots OH/H_2O$. Moreover, this process clearly brought forward that the H^+-US/CI/Fe^0 system provided an effective preparation method for directional oxidation from PMSO to $PMSO_2$.

3.5.2. Transformation

Consequently, the results further indicated that produced HVI-oxo species and ClO_2 exhibited a certain transforming relationship. Previously, Fabian and Gordon proposed the formation of $FeClO_2^{2+}$ (Fe^{3+} + ClO_2^-) intermediates, but they did not deny the existence of Fe^{IV} [24–26]. According to $FeClO_2^{2+}$, Wang et al. proposed the combination of "Fe^{2+} + ClO_2", which involved the reduction of ClO_2 to ClO_2^- by aqueous Fe^{II}. This proceeded by both outer-sphere (86%) and inner-sphere (14%) electron-transfer pathways [27]. Moreover, the traditional mainstream views of the catalysis of ClO_2^- by metalloporphyrin or Clds were as follows (considering Fe-Pors as an example, Scheme 1), heterolytic (Route 1, to obtain Compound I [$Por^{+\bullet}\cdots Fe^{IV}$=O] and hypochlorite (HOCl/$^-$OCl)) and homolytic (Route 2, to obtain chlorine monoxide (ClO•) and Compound II [$Por\cdots Fe^{IV}$=O]) cleavage of ClO_2^- [10,11].

Recently, a study used the natural substrate, ClO_2^-, and the model substrate, PAA, under x-Cld role to reveal the formation of distinct intermediates; i.e., the transient triplet-state biradical species distinct from Compound I and Compound II [11]. Moreover, the studies also offered convenient routes to produce ClO_2 in water by catalyzing ClO_2^- via non-heme Fe^{III}- or $Mn^{II/III}$-complexes. The processes underwent the proton-coupled electron transfer (Mn^{II}) [2] or initiated the formation of high-valent Fe and Mn^{IV}–OH intermediates with oxidant PAA (Mn^{III}) [18].

However, combined with the identifications in this study and based on the analogy of ClO_2^- catalysis of Mn^{II}-complexes [2], a possible Fe^0 catalytic mechanism for ClO_2^- to form interdependent high-valent-Fe-oxo and ClO_2 was proposed under protonation (Scheme 2). The proposed Fe^0 catalytic mechanism also involved Fe^{II} and Fe^{III} activation processes. Relying on the role of H^+, the surface corrosion of Fe^0 to form ionic Fe led to interfacial catalysis, and then the ultrasonic field provided the driving force for the mass transfer to undergo diffuse catalysis (a transition process from interfacial catalysis to liquid phase (bulk phase) catalysis). Furthermore, the ultrasonic cavitation could provide the activation of $HClO_2$ to produce ClO_2 and polish the surface of Fe^0 to continuously expose fresh Fe^0 sources (Fig. 2). Scheme 2 presented that the ions release of Fe^0 led to subsequent chain transfer processes of $[Fe^{II}(H_2O)_6]^{2+}$ [51] and $[HO-Fe^{III}(H_2O)_5]^{2+}$, which sourced from the hydrolysis of $[Fe^{III}(H_2O)_6]^{3+}$ [52,53]. Direct addition of Fe^{II} and Fe^{III} afforded the pseudo-second-order kinetics dependence, while Fe^0 expressed the pseudo-1.5-order kinetics dependence after the ion accumulation stage (0–7 min, Fig. 1b), which indicated that the ion leaching of Fe^0 affected reaction equilibrium. The as-formed HVI-oxo species, $O=Fe^{IV}$ or $[O=Fe^{IV}]^{\bullet+}$, corresponding to the catalytic transfer station: one pathway generated ClO_2, which involved protonation of the oxo ligand on Fe^{IV} and thus accounted for the observed pH dependence (pH with great effect) for ClO_2 production (Fig. 5c) [2]. Other pathways led to the formation of ClO_3^- and Fe^{II}, which rapidly reacted with ClO_2 to form $[HO-Fe^{III}]^{2+}$, thus re-entering the catalytic cycle [2] (macroscopically being consistent with the process: $Fe^{2+} + ClO_2 \rightarrow FeClO_2^{2+} \rightarrow Fe^{3+} + ClO_2^-$ [24–26]). The dominant species, namely, $[HO-Fe^{III}]^{2+}$, reacted with ClO_2^- in the presence of protons via homolytic Cl–O bond cleavage to form ClO• and regenerate the $O=Fe^{IV}$ species or via heterolytic Cl–O bond cleavage to form ClO^- and regenerate the $[O=Fe^{IV}]^{\bullet+}$ species [2,10]. The generated ClO• or ClO^- with strong reactivity entered reaction toward the low-valence Cl^-. Furthermore, the previous research also reported and supported that the $[Fe^{II}(H_2O)_6]^{2+}$ under HClO could allow the production of $O=Fe^{IV}$ [54].

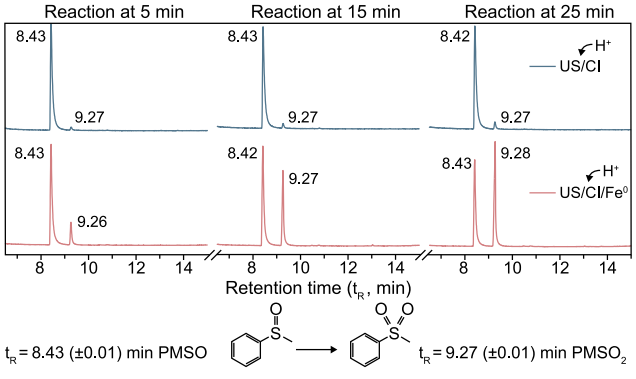

Fig. 6. Comparisons of GC/MS detection with PMSO as a chemical probe: PMSO dosage (0.3 mM); other conditions ibid., Fig. 1.

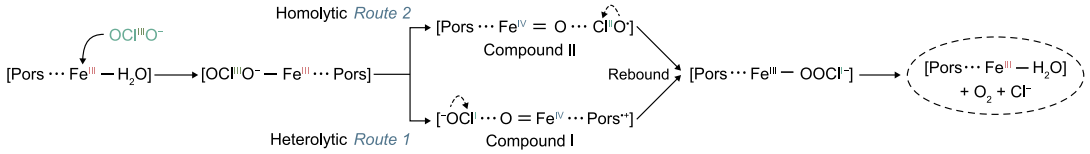

Scheme 1. The possible mechanisms of ClO_2^- cleavage.

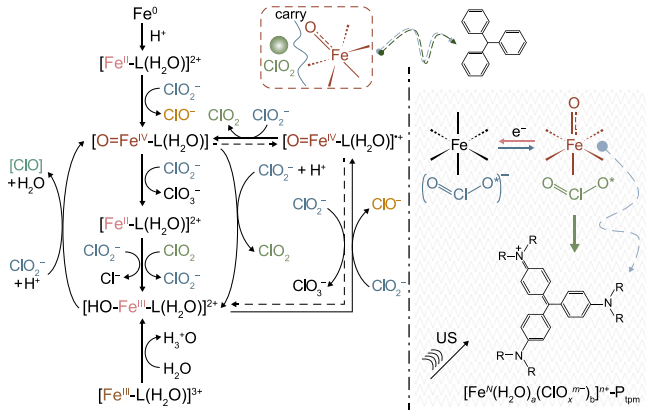

Scheme 2. Proposed reaction mechanism for Fe_b-activated ClO_2^- by the role of protonation.

3.5.3. Action

All these abovementioned catalysis/activation processes were based on Fe_b and ClO_2^-; therefore, how to relate to the degradation process for removing contaminants?

In contrast, with iron-free catalysis, the H^+-US/CI system for pollutant removal underwent autocatalysis due to the formation process of ClO_2. Kieffer and Gordon reported that Cl^- could catalyze the disproportionation of $HClO_2$ [31]. Cl^- could alter the reaction from equation (5) to equation (28) [31]. Furthermore, Horvath et al. considered that the autocatalysis concerning H^+, Cl^-, and key intermediate, HOCl, led to the unique redox reaction [55]. Olagunju et al. reported that ClO_2 production after the induction period was due to the reaction of the intermediate HOCl species with ClO_2^- [56]. The apparent piecewise and non-integer kinetics observed in this study also supported the abovementioned result. The accumulation of intermediates, Cl^- or ClO^- led to a self-catalyzed reaction to boost the yield of ClO_2, following the "S"-curve of the removal process by using the H^+-US/CI system (Fig. 1a). Attention: in general, purity of commercial sodium chlorite is around 80%, which is accompanied by part of chloride ions; therefore, the commodity might have itself contributed to autocatalysis.

$$4ClO_2^- + 2H^+ \rightarrow ClO_3^- + Cl^- + 2ClO_2 + H_2O \quad (28)$$

However, in terms of the H^+-US/CI/Fe_b system, the coordination catalysis, i.e., effective contact catalysis/activation, could be proposed based on the abovementioned analyses presented in sections 3.5.1 and 3.5.2. The as-formed coordination center $[Fe^N(H_2O)_x]^{n+}$ could be obtained by complexation of reactive intermediates such as ClO_2 (ClO_2^-) or ClO^- by substituting H_2O, and its valence state could also be affected to form the possible $[Fe^N(H_2O)_a(ClO_x^{m-})_b]^{n+}$ complex, briefly, $Fe^NClO_x^{M+}$ species. This process could be analogous to hemoglobin carrying oxygen, which could act as one transmission type. The $[Fe^N(H_2O)_x]^{n+}$ could carry ClO_2 throughout the liquid phase to increase the chance of collision or contact among the molecules, particularly when driven by the US. Owing to the abovementioned coordination, the solute contaminant macromolecules were caught by the water molecules with intermolecular forces (similarly, pollutant molecules were trapped by the friction) to form localized/limited catalysis or activation, namely, $[Fe^N(H_2O)_a(ClO_x^{m-})_b]^{n+}$-$P_{tpm}$ complexes, which easily led to the outer-sphere and inner-sphere electron transfers. Furthermore, the processes of free radical and non-free radical oxidation and active species for removing contaminants could all be produced. The above-mentioned catalytic processes were generally selective for contaminant structures.

4. Conclusions

(1) The system, namely, Fe_b activating protonated ClO_2^-, could be utilized to synchronously remove inorganic ions (ClO_2^-) and organic pollutants (tpm-derivatives) by interdependent high-valent-Fe-oxo and ClO_2. However, the redox system presented selective oxidation rather than non-selective oxidation for contaminants removal.

(2) Differences were observed between metal porphyrin/complexes and ion catalysis. Fe_b-induced activation of protonated ClO_2^- seemed to approach Mn-porphyrin/complexes catalysis of ClO_2^-; both processes produced ClO_2. In contrast, Fe-Cld/porphyrin catalysis more tended to catalyze ClO_2^- to produce Cl^- and O_2.

(3) Interestingly, this study further provided the preparation methods of two products, i.e., ClO_2 and sulfones. The Fe_b-activated ClO_2^- could correspond to a method of oriented oxidation of sulfoxides to sulfones and environmentally allow for ClO_2 preparation for the on-site use (e.g., disinfection or sterilization) and further ClO_2 production.

(4) Owing to the micro/small dosage of activators used in this study, the autocatalytic process became explicit. In general, the studies were based on a high dosage of activators or homogeneous activation except for the autocatalysis caused by the pollutant structures (e.g., hydroquinone or benzoquinone), which shortened the autocatalytic accumulation processes. However, it has also made a preliminary exploration for the controlled release-catalysis of ionic Fe with small/micro dosages.

Declaration of competing interest

The authors declare that they have no known competing financial interests or personal relationships that could have appeared to influence the work reported in this paper.

Acknowledgements

This work was supported by the State Key Laboratory of Urban Water Resource and Environment, Harbin Institute of Technology (2019DX08), National Natural Science Foundation of China (52100036), Natural Science Foundation of Shan-dong Province of China (ZR20210E119), Open Project of State Key Laboratory of Urban Water Resource and Environment, Harbin Institute of

Technology (QA202140), and Scientific Research Foundation of Harbin Institute of Technology at Weihai (HIT(WH)2019).

Moreover, the first author is deeply grateful to his late father (Biao Xu)!

References

[1] R.L. Hao, X.Z. Mao, Z. Qian, Y. Zhao, L.D. Wang, B. Yuan, K.M. Wang, Z.H. Liu, M. Qi, J. Crittenden, Simultaneous removal of SO_2 and NO using a novel method of ultraviolet irradiating chlorite-ammonia complex, Environ. Sci. Technol. 53 (2019) 9014–9023.
[2] S.D. Hicks, D. Kim, S.L. Xiong, G.A. Medyedey, J. Caruthers, S. Hong, W. Nam, M.M. Abu-Omar, Non-heme manganese catalysts for on-demand production of chlorine dioxide in water and under mild conditions, J. Am. Chem. Soc. 136 (2014) 3680–3686.
[3] H. Cosson, W.R. Ernst, Photodecomposition of chlorine dioxide and sodium-chlorite in aqueous-solution by irradiation with ultraviolet-light, Ind. Eng. Chem. Res. 33 (1994) 1468–1475.
[4] S.R. Huang, W.H. Gan, M.Q. Yan, X.R. Zhang, Y. Zhong, X. Yang, Differential UV-vis absorbance can characterize the reaction of organic matter with ClO_2, Water Res. 139 (2018) 442–449.
[5] S. Navalon, M. Alvaro, H. Garcia, Reaction of chlorine dioxide with emergent water pollutants: Product study of the reaction of three β-lactam antibiotics with ClO_2, Water Res. 42 (2008) 1935–1942.
[6] V. Rouge, S. Allard, J.P. Croue, U. von Gunten, In situ formation of free chlorine during ClO_2 treatment: Implications on the formation of disinfection byproducts, Environ. Sci. Technol. 47 (2018) 13421–13429.
[7] A. Katz, N. Narkis, Removal of chlorine dioxide disinfection by-products by ferrous salts, Water Res. 35 (2001) 101–108.
[8] Standards for Drinking Water Quality, GB 5749–2022.
[9] J.A. Mayfield, B. Blanc, K.R. Rodgers, G.S. Lukat-Rodgers, J.L. DuBois, Peroxidase-type reactions suggest a heterolytic/nucleophilic O-O joining mechanism in the heme-dependent chlorite dismutase, Biochemistry 52 (2013) 6982–6994.
[10] I. Schaffner, G. Mlynek, N. Flego, D. Puhringer, J. Libiseller-Egger, L. Coates, S. Hofbauer, M. Bellei, P.G. Furtmuller, G. Battistuzzi, G. Smulevich, K. Djinovic-Carugo, C. Obinger, Molecular mechanism of enzymatic chlorite detoxification: Insights from structural and kinetic studies, ACS Catal. 7 (2017) 7962–7976.
[11] J. Puschmann, D. Mahor, D.C. de Geus, M.J.F. Strampraad, B. Srour, W.R. Hagen, S. Todorovic, P.L. Hagedoorn, Unique biradical intermediate in the mechanism of the heme enzyme chlorite dismutase, ACS Catal. 11 (2021) 14533–14544.
[12] A.Q. Lee, B.R. Streit, M.J. Zdilla, M.M. Abu-Omar, J. DuBois, Mechanism of and exquisite selectivity for O-O bond formation by the heme-dependent chlorite dismutase, Proc. Natl. Acad. Sci. U.S.A. 105 (2008) 15654–15659.
[13] J.M. Keith, M.M. Abu-Omar, M.B. Hall, Computational investigation of the concerted dismutation of chlorite ion by water-soluble iron porphyrins, Inorg. Chem. 50 (2011) 7928–7930.
[14] M.J. Zdilla, A.Q. Lee, M.M. Abu-Omar, Concerted dismutation of chlorite ion: Water-soluble iron-porphyrins as first generation model complexes for chlorite dismutase, Inorg. Chem. 48 (2009) 2260–2268.
[15] M.J. Zdilla, A.Q. Lee, M.M. Abu-Omar, Bioinspired dismutation of chlorite to dioxygen and chloride catalyzed by a water-soluble iron porphyrin, Angew. Chem. Int. Ed. 47 (2008) 7697–7700.
[16] T.P. Umile, J.T. Groves, Catalytic generation of chlorine dioxide from chlorite using a water-soluble manganese porphyrin, Angew. Chem. Int. Ed. 50 (2011) 695–698.
[17] S.D. Hicks, J.L. Petersen, C.J. Bougher, M.M. Abu-Omar, Chlorite dismutation to chlorine dioxide catalyzed by a water-soluble manganese porphyrin, Angew. Chem. Int. Ed. 50 (2011) 699–702.
[18] T.B. Champ, J.H. Jang, J.L. Lee, G. Wu, M.A. Reynolds, M.M. Abu-Omar, Lignin-derived non-heme iron and manganese complexes: Catalysts for the on-demand production of chlorine dioxide in water under mild conditions, Inorg. Chem. 60 (2021) 2905–2913.
[19] Z. Wang, W. Qiu, S.Y. Pang, Q. Guo, C.T. Guan, J. Jiang, Aqueous iron(IV)-oxo complex: An emerging powerful reactive oxidant formed by iron(II)-based advanced oxidation processes for oxidative water treatment, Environ. Sci. Technol. 56 (2022) 1492–1509.
[20] K.J. Hou, P. Shen, Z. Wang, Z.J. Pi, F. Chen, X.M. Li, H.R. Dong, Q. Yang, Revisiting the contribution of $Fe^{IV}O^{2+}$ in Fe(II)/peroxydisulfate system, Chin. Chem. Lett. (2022).
[21] G.H. Hurst, W.R. Knocke, Evaluating ferrous iron for chlorite ion removal, J. Am. Water Works Ass. 89 (1997) 98–105.
[22] A. Iatrou, W.R. Knocke, Removing chlorite by the addition of ferrous iron, J. Am. Water. Works Ass. 84 (1992) 63–68.
[23] G. Schmitz, H. Rooze, Reaction-mechanisms of chlorite and chloride dioxide .3. The disproportionation of chlorite, Can. J. Chem. 63 (1985) 975–980.
[24] I. Fabian, G. Gordon, Kinetics and mechanism of the complex formation of the chlorite ion and iron(III) in aqueous solution, Inorg. Chem. 30 (1991) 3994–3999.
[25] I. Fabian, G. Gordon, Iron(III)-Catalyzed decomposition of the chlorite ion: An inorganic application of the quenched stopped-flow method, Inorg. Chem. 31 (1992) 2144–2150.
[26] I. Fabian, R. van Eldik, Complex-Formation kinetics of iron(III) with chlorite ion in aqueous solution. Mechanistic information from pressure effects, Inorg. Chem. 32 (1993) 3339–3342.
[27] L. Wang, I.N. Odeh, D.W. Margerum, Chlorine dioxide reduction by aqueous iron(II) through outer-sphere and inner-sphere electron-transfer pathways, Inorg. Chem. 43 (2004) 7545–7551.
[28] Q.H. Xu, H. Zhang, H.R. Leng, H. You, Y.H. Jia, S.T. Wang, Ultrasonic role to activate persulfate/chlorite with foamed zero-valent-iron: Sonochemical applications and induced mechanisms, Ultrason. Sonochem. 78 (2021), 105750.
[29] IARC Monographs Vol 129 group, Carcinogenicity of gentian violet, leucogentian violet, malachite green, leucomalachite green, and CI Direct Blue 218, Lancet Oncol. 22 (2021) 585–586.
[30] T. Lehtimaa, V. Tarvo, G. Mortha, S. Kuitunen, T. Vuorinen, Reactions and kinetics of Cl(III) decomposition, Ind. Eng. Chem. Res. 47 (2008) 5284–5290.
[31] R.G. Kieffer, G. Gordon, Disproportionation of chlorous acid, I. Stoichiometry. Inorg. Chem. 7 (1968) 235–239.
[32] Q.H. Xu, Z.P. Li, H. You, S.T. Wang, H.Y. Li, Magnetically separable Fe-base deposited on different carbon sources for ultrasound/persulfate-like heterogeneous activation: Optimized synthesis and field driving process, Chemosphere 298 (2022), 134270.
[33] M.C. Taylor, J.F. Whitte, G.P. Vincent, G.I. Cunnigham, Sodium chlorite properties and reactions, Ind. Eng. Chem. 32 (1940) 899–903.
[34] E.M. Rodriguez, A. Rey, E. Mena, F.J. Beltran, Application of solar photocatalytic ozonation in water treatment using supported TiO_2, Appl. Catal. B Environ. 254 (2019) 237–245.
[35] G.V. Buxton, C.L. Greenstock, W.P. Helman, A.B. Ross, Critical review of rate constants for reactions of hydrated electrons hydrogen-atoms and hydroxyl radicals (•OH/•O$^-$) in aqueous-solution, J. Phys. Chem. Ref. Data 17 (1988) 513–886.
[36] H. Bataineh, O. Pestovsky, A. Bakac, pH-induced mechanistic changeover from hydroxyl radicals to iron(IV) in the Fenton reaction, Chem. Sci. 3 (2012) 1594–1599.
[37] C. Tai, X.X. Gu, H. Zou, Q.H. Guo, A new simple and sensitive fluorometric method for the determination of hydroxyl radical and its application, Talanta 58 (2002) 661–667.
[38] N. Imaizumi, T. Kanayama, K. Oikawa, Effect of dimethylsulfoxide as a masking agent for aqueous chlorine in the determination of oxychlorines, Analyst 120 (1995) 1983–1987.
[39] Z.L. Jiang, S.M. Zhou, A.H. Liang, C.Y. Kang, X.C. He, Resonance scattering effect of rhodamine dye association nanoparticles and its application to respective determination of trace ClO_2 and Cl_2, Environ. Sci. Technol. 40 (2006) 4286–4291.
[40] P. Neta, R.E. Huie, A.B. Ross, Rate constants for reactions of inorganic radicals in aqueous solution, J. Phys. Chem. Ref. Data 17 (1988) 1027–1284.
[41] S. Kepler, M. Zeller, S.V. Rosokha, Anion-π complexes of halides with *p*-benzoquinones: Structures, thermodynamics, and criteria of charge transfer to electron transfer transition, J. Am. Chem. Soc. 141 (2019) 9338–9348.
[42] R.Z. Chen, J.J. Pignatello, Role of quinone intermediates as electron shuttles in Fenton and photoassisted Fenton oxidations of aromatic compounds, Environ. Sci. Technol. 31 (1997) 2399–2406.
[43] F.B. Li, X.Z. Li, C.S. Liu, X.M. Li, T.X. Liu, Effect of oxalate on photodegradation of bisphenol a at the interface of different iron oxides, Ind. Eng. Chem. Res. 46 (2007) 781–787.
[44] S. Seibig, R. van Eldik, Kinetics of [Fe^{II}(edta)] oxidation by molecular oxygen revisited. New evidence for a multistep mechanism, Inorg. Chem. 36 (1997) 4115–4120.
[45] H.H. Awad, D.M. Stanbury, Electron transfer between azide and chlorine dioxide: The effect of solvent barrier nonadditivity, J. Am. Chem. Soc. 115 (1993) 3636–3642.
[46] M.R. Grace, T.W. Swaddle, Kinetics of reactions of aqueous iron(III) ions with azide and thiocyanate at high pressures, Inorg. Chem. 31 (1922) 4674–4678.
[47] M. Soulard, F. Bloc, A. Hatterer, Diagrams of existence of chloramines and bromamines in aqueous solution, J. Chem. Soc. Dalton Trans. 12 (1981) 2300–2310.
[48] J. Wenk, M. Aeschbacher, E. Salhi, S. Canonica, U. von Gunten, M. Sander, Chemical oxidation of dissolved organic matter by chlorine dioxide, chlorine, and ozone: Effects on its optical and antioxidant properties, Environ. Sci. Technol. 47 (2013) 11147–11156.
[49] A.V. Kutchin, S.A. Rubtsova, I.V. Loginova, Reactions of chlorine dioxide with organic compounds - Selective oxidation of sulfides to sulfoxides by chlorine dioxide, Russ. Chem. Bull. 50 (2001) 432–435.
[50] A.V. Kutchin, S.A. Rubtsova, D.V. Sudarikov, M.Y. Demakova, Chlorine dioxide in chemo- and stereoselective oxidation of sulfides, Russ. Chem. Bull. 62 (2013) 1–5.
[51] L. Guimaraes, H.A. de Abreu, H.A. Duarte, Fe(II) hydrolysis in aqueous solution: A DFT study, Chem. Phys. 333 (2007) 10–17.
[52] R.L. Martin, P.J. Hay, L.R. Pratt, Hydrolysis of ferric ion in water and conformational equilibrium, J. Phys. Chem. A 102 (1998) 3565–3573.
[53] H.A. de Abreu, L. Guimaraes, H.A. Duarte, Density-functional theory study of

iron(III) hydrolysis in aqueous solution, J. Phys. Chem. A 110 (2006) 7713–7718.
[54] S. Liang, L.Y. Zhu, J. Hua, W.J. Duan, P.T. Yang, S.L. Wang, C.H. Wei, C.S. Liu, C.H. Feng, Fe^{2+}/HClO reaction produces $Fe^{IV}O^{2+}$: An enhanced advanced oxidation process, Environ. Sci. Technol. 54 (2020) 6406–6414.
[55] A.K. Horvath, I. Nagypal, I.R. Epstein, Three autocatalysts and self-inhibition in a single reaction: A detailed mechanism of the chlorite-tetrathionate reaction, Inorg. Chem. 45 (2006) 9877–9883.
[56] O. Olagunju, P.A. Siegel, R. Olojo, R.H. Simoyi, Oxyhalogen-sulfur chemistry: Kinetics and mechanism of oxidation of N-acetylthiourea by chlorite and chlorine dioxide, J. Phys. Chem. A 110 (2006) 2396–2410.